Current technological state of radiation therapy for the treatment of lung cancer

***Authors**

Sina Mossahebi, Ph.D.
Department of Radiation Oncology
University of Maryland School of Medicine
Baltimore, MD USA

Chaitanya Kalavagunta, Ph.D.
Department of Radiation Oncology
University of Maryland School of Medicine
Baltimore, MD USA

Heeteak Chung, Ph.D.
Department of Radiation Oncology
University of Maryland School of Medicine
Baltimore, MD USA

Corresponding Author:
Heeteak Chung, Ph.D.
Department of Radiation Oncology
University of Maryland, Baltimore
850 W. Baltimore Street
Baltimore, MD, 21201
Phone: 410-369-5323
FAX: 410-347-0870
E-mail: hchung@umm.edu

Conflict of Interest: None

ABSTRACT

The field of radiation therapy has come a long way since the discovery of the x-ray in 1895 by Wilhelm Rogentgen. In less than a year after its discovery, x-ray was used in medical applications. After over a century of usage and advancements, x-ray has become a staple of diagnostic and therapeutic medical applications. Likewise, radiation therapy has benefited from the advancements in diagnostic and therapeutic applications especially for the treatment of lung cancers. Due to the unique nature of the lung tumors (e.g., tumor movements), the treatment of lung cancer utilizes several technologies that facilitate treatment delivery in terms of treatment modality and imaging. This review provides a general overview of the radiation treatment machines and technologies used in the clinic for the treatment of lung cancer.

1. Introduction

In the United States, it was estimated that 848,200 new cancer cases for males and 810,170 new cases for females would be reported in 2015 (Society, 2015). It was estimated that 221,000 new lung cases (both males and females) are expected in the same year, which accounts for approximately 13% of all cancer diagnosed in the United States. However, lung cancer accounts for more deaths than any other cancer for both men and women. It was estimated that 158,040 deaths are expected in 2015, which accounts for approximately 27% of all cancer deaths. Even though the death rates have begun to decline since the 1990's, lung cancer is still considered as one of the deadliest cancer in the United States. In Europe, the incident of lung cancer for male and female was 15.9% and 7.4%, respectively in 2012.(Ferlay et al., 2013) The reported deaths from the disease for male and female were 26.1% and 12.7%, respectively. In total, lung cancer accounted for 353,000 deaths, which was one fifth of the total deaths in Europe.

Despite significant improvements and advances in treatment technology and options, survival from this disease is still poor, especially for locally advanced and metastatic lung cancer. Recently, a randomized phase 3 trial of chemoradiation and various sequence for stage III non-small cell lung cancer showed the median survival times of 14.6, 17.0, and 15.6 months for sequential chemotherapy and radiation, concurrent chemotherapy and radiation, and concurrent chemotherapy and twice daily radiation, respectively (Curran et al., 2011). For the metastatic non-small cell lung cancer, the median survival was approximately 8 months.(Lee et al., 2012) Lastly, a recent study (Chang et al., 2015) where 58 patients were randomized to either stereotactic ablative radiotherapy (SABR) group or surgery group with patients with an inoperative stage I non-small cell lung cancer has shown promising results. The radiotherapy group showed an estimated overall survival at 3 years of 95% compared with 79% in the surgery group.

While the prognostication for advanced and metastatic lung cancers may be poor, early stage lung cancers do have very promising outcome. Among many reasons for such improvements in the outcome for early stage lung cancers, one driving force is the technological advances in the radiation therapy. Historically, the first radiotherapy was performed by placing a radioactive isotope in the tumor. However, this posed a

significant risk of damaging the lung during the insertion process. To avoid such invasive procedures, a kilo-voltage x-ray was used to treat the cancer. Unfortunately, the kilo-voltage x-ray showed to be too low of an energy and deposited high doses to the skin while not enough radiation to the tumor. To spare the skin, a mega-voltage x-ray was introduced which is the current standard of practice for the treatment of lung cancer. Recently, there has been surge of interest in using particle therapy (e.g., protons) to treat lung cancers. In addition to improvements to the treatment modalities, other technological advancements in the area of imaging, 3D/4D patient and tumor modeling, and treatment plan delivery has significantly improved the treatment outcome of our patients.

2. Computed Tomography

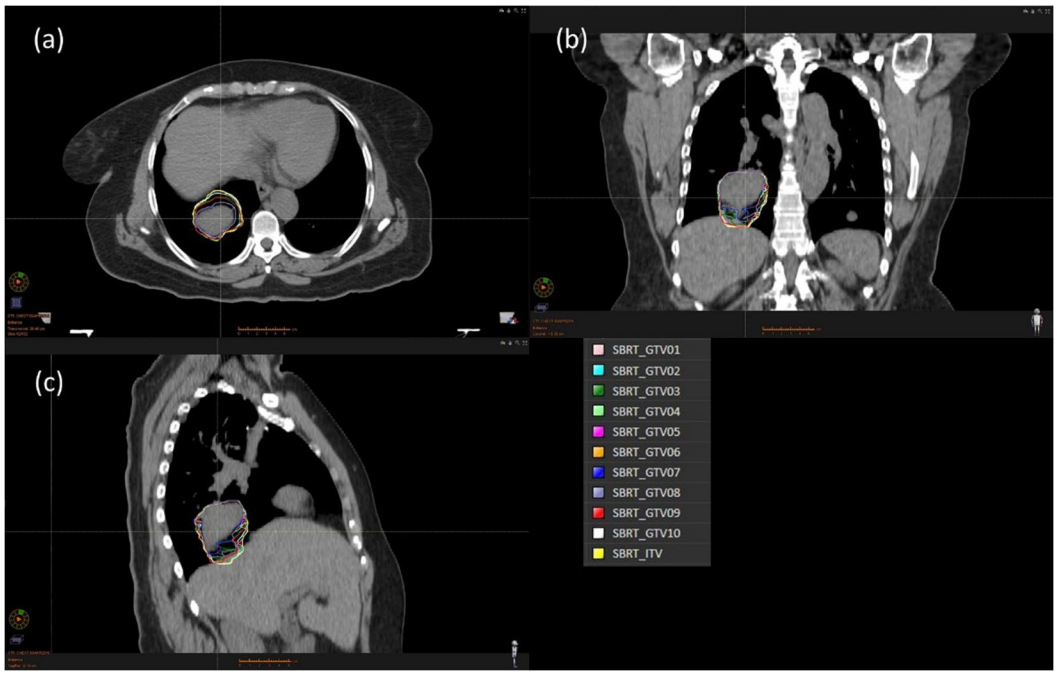

Figure 1. CT images of a lung cancer. (a) Transvers, (b) Coronal, (c) Sagittal, and (d) contour legend. The 11 contours shown in all three images indicate the 10-phases of breathing pattern with the 11th contour being the union of all 10-phases, which indicates the full range of motion of the tumor. The 10-phase breathing patter was obtained using 4DCT.

Computed tomography (CT) simulation is the pre-treatment process to determine the location, shape, and size of the tumor with respect to the patient's anatomy to be treated. During the simulation, the patient is positioned on the CT table using

immobilization devices to maintain the position of the patient at the time of the treatment the way he/she was positioned on the CT table. Computed tomography also provides the physical properties of the patient's anatomy that will later be used in a treatment planning system (TPS) to calculate the radiation dose. The CT images are used by TPS to design the best treatment plan for the patient. The short acquisition time of the CT compared to other imaging modalities such as, magnetic resonance imaging (MRI) and positron emission tomography (PET) helps to better manage the tumor motion. However, to take advantage of the metabolic information available from MRI and PET, it is very common practice to merge the CT images with MRI and/or PET for tumor delineation (Ahn & Garg, 2008; Glatstein, Lichter, Fraass, Kelly, & van de Geijn, 1985; Mak, Corry, Lau, Rischin, & Hicks, 2011; Simpson et al., 2009).

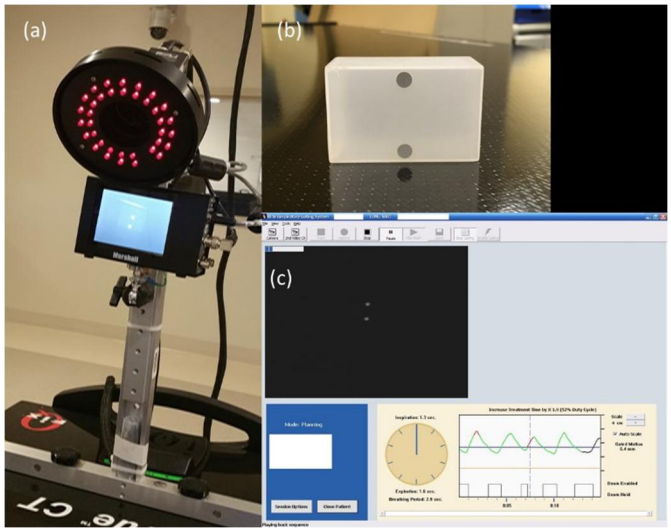

Figure 2. Infrared tracking system (a) Infrared tracking camera, (b) Infrared reflective block, and (c) graphic user interface

Respiratory motion can cause tumor to move out of the radiation field, increase the apparent size of the tumor in the image (McCarter & Beckham, 2000), and poses an increased irradiation of normal tissues. To mitigate the tumor motion from respiration, it is important to understand the magnitude and the direction of the motion. This can be done by using a 4-dimensional computed tomography (4DCT). Four-dimensional computed tomography acquires large number of individual CT scans at various respiratory phases (Keall et al., 2006; Webb, 2006) that can provide a visual representation of the tumor motion during a normal breathing cycle. With this

information, a clinician can create a target volume in the treatment planning system that will cover the full range of motion of the tumor (Figure 1). During the image acquisition of 4DCT, the breathing phase can be tracked in two methods. The first method is the infrared (IR) system where an infrared tracking camera and a reflective block are used to monitor the patient's respiratory motion real time (Figure 2). The digital camera is focused on the reflective block with the infrared reflectors, which is placed on the patient's abdomen. The movement of the infrared reflectors provides an information about the patient's breathing patter in a sinusoidal waveform (Vedam et al., 2003) that can be imported to the CT scanner to process the 4DCT image data set. The second method is the pneumatic belt system called bellows, which also tracks the patient's respiratory motion. The device consists of a rubber air bellows that is attached to a pressure transducer and detects the air pressure changes from the patients' breathing. The air pressure variations are converted to a voltage signal in a waveform which is used by the 4DCT for image processing (Glide-Hurst, Schwenker Smith, Ajlouni, & Chetty, 2013).

To further mitigate the tumor motion, a breath hold technique called respiratory gating can be used. This is a technique where the patient holds his/her breath to reduce the magnitude of the tumor motion. While the patient holds his/her breathe, 4DCT scan would be done to characterize the tumor motion during the breath hold. Similar to free breathing 4DCT, both the infrared system and the bellows system can help the patient hold their breath in a reproducible manner. The respiratory gated 4DCT can also be used to create a target volume of the tumor. The respiratory gating technique has shown it can reduce the motion and the target volume (Shen et al., 2003). Limiting the tumor movement by breath holding or tracking tumor motion by respiratory gating methods can significantly reduce the normal lung volume (Barnes et al., 2001; Rosenzweig et al., 2000).

3. Treatment Planning

Treatment planning in radiation oncology can be described as the selection of parameters that are most optimal for the radiation treatment of a cancer of interest (e.g., lung tumor). These parameters include the delineation of the target and organs at risk, dose prescription and distribution, patient positioning and treatment machine

settings (Khan & Gerbi, 2011). A treatment planning system is a computer program that simulates the interactions of a set of radiation beams with the patient and the information workflow is laid out in figure 3 (Pawlicki, Scanderbeg, & Starkschall, 2016). Currently, there are several commercially available treatment planning systems. While they may have differences in specific features, they all simulate the radiation treatment (Figure 4).

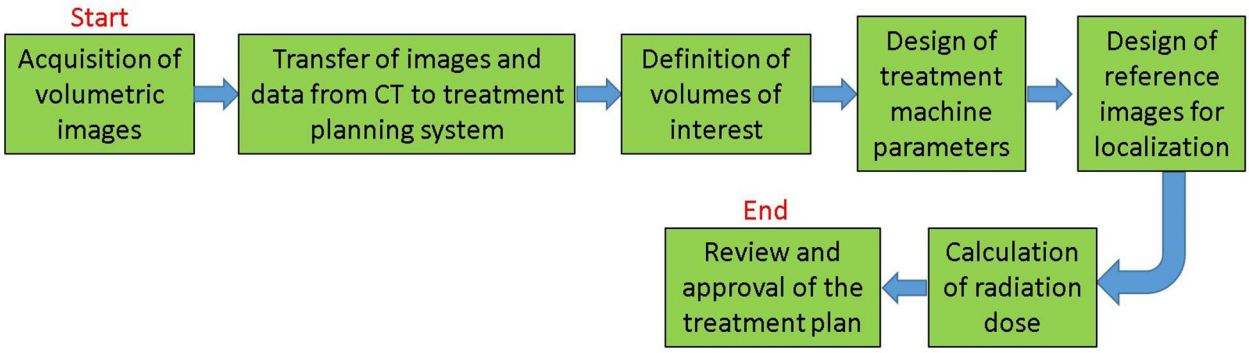

Figure 3. Treatment planning workflow

Figure 4. A commercially available treatment planning system used in radiation therapy

The target volume is composed of multiple layers of margins. It starts with the visible tumor or gross tumor volume (GTV) from the CT image set. The first margin from the GTV is the internal target volume (ITV) which accounts for the tumor motion. Once the ITV is established, the clinical tumor volume (CTV) is created accounting for the

microscopic extension around the GTV. Lastly, the planning tumor volume (PTV) is created accounting for the uncertainties in the patient movement and setup (International Commission on Radiation & Measurements, 1999). Additional margins may be added around the target volume to account for the limitations of the treatment technique. The minimum target dose is represented by a dose "cloud" of the prescribed dose covering the PTV.

The organs at risk (OAR) are the critical structures near the target volume where the radiation dose to them cannot exceed certain limit. In order to safely deliver dose to the target volume while minimizing dose to the OARs, additional margins may be added to the OARs. Furthermore, the prescribed dose to the PTV may be lowered in order to limit the dose to the OARs (e.g., spine cannot exceed radiation dose of 50 Gy). The prescribed dose is related to the treatment site, the energy of the radiation, dose per fraction, number of fractions and total dose (Gunderson & Tepper, 2015). Patient positioning is done using immobilization devices that reproducibly position the patient established at the time of the CT simulation. Target localization techniques use information obtained at the time of the CT simulation to accurately position the patient. The dose distribution of the target and OARs are evaluated by the clinicians to determine the clinical acceptability of the radiation plan for the actual treatment.

The organs at risk for the treatment of the lung tumor are liver, brachial plexus, stomach, kidneys, spinal cord, heart, esophagus, skin and lung(s). The main concern in lung tumors is the respiratory motion that can lead to inaccurate target definition in treatment planning and subsequent underdose of the target and/or overdose of the organs at risk during treatment delivery (Li, 2011). Patients are typically simulated in supine position with arms above the head. Individual tumor motion is assessed for most patients using 4DCT. The magnitude of the setup uncertainity depends upon the use of on-board image guidance systems. Depending on the availability/unavailability of daily image guidance used, an isotropic margin of several millimeters can be added to the CTV to obtain the PTV respectively. The patient can be planned on a free breathing scan however; average CT scan from the 4DCT can be used for planning purpose.

The treatment planning system uses a model-based algorithm to compute the dose distribution with a physical model that simulates the actual radiation transport. The most popular model-based dose calculation algorithm currently available in the market is the convolution-superposition algorithm (Ahnesjo & Aspradakis, 1999). In radiation therapy, the radiation that interacts with the materials (e.g., patient) can be considered as a primary and scatter x-ray. The primary x-ray is the x-ray that did not undergo any scatter. The scatter x-ray is the x-ray that did undergo some type of scatter in the materials. The convolution-superposition algorithm considers the radiation interaction of the primary and scattered x-rays separately. The transport of the primary x-rays are the product of the attenuation coefficient and primary energy fluence. The attenuation coefficient (probability of the x-ray interacting with matter in unit length) of the primary x-rays are obtained from the CT information. The scattered x-rays are from the Monte Carlo simulation in homogeneous water. The product sum of these two components (i.e., primary and scattered x-rays) would provide the dose distribution. In addition to attenuation coefficient, the CT data set also provides internal geometric anatomy of the patient for heterogeneity consideration.

Although CT images can distinguish between anatomic structures with different voxel intensity, they have limited use in discriminating between soft tissue structures. For this reason, it is common to register MR and/or PET images with CT in the treatment planning system to improve target delineation. Positron Emission Tomography (PET) is based on the principle of determination of 3D distribution of positron emitter radionuclide in the body. It provides functional information, which can be used for cancer staging. PET-CT scanners have been constructed that can simultaneously acquire PET and CT images on the same machine with unchanged patient positioning (Levitt, 2012). Information from PET images can thus be used for delineation of lung GTVs by using rigid image registration with CT. MRI images have high resolution, excellent soft tissue contrast and can provide additional functional information with techniques like diffusion weighted, and dynamic contrast enhanced imaging.

4. Medical Linear Accelerator and Other Treatment Machines

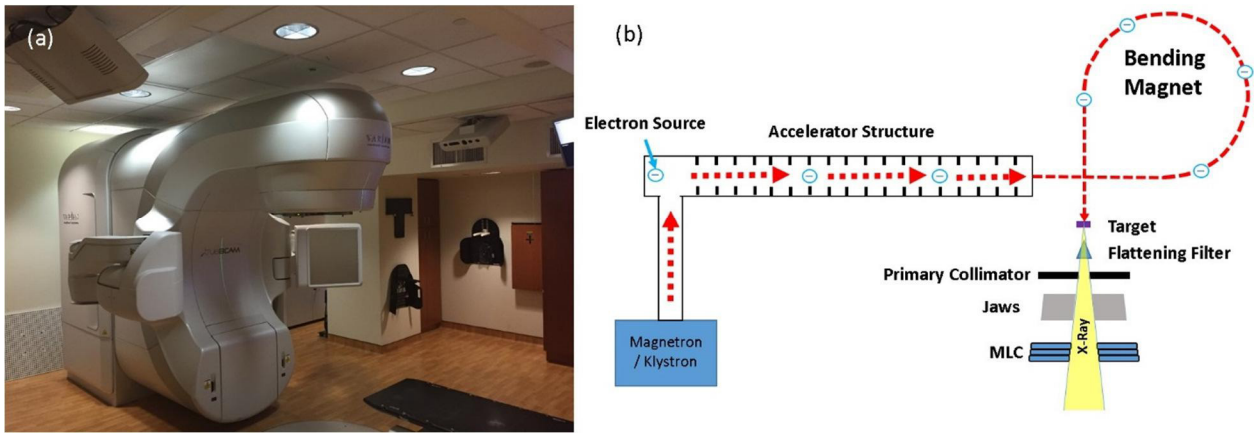

Figure 5: (a) Megavoltage (MeV) medical linear accelerator (b) Illustration of the operation of medical linear accelerator

The technological improvements made in the current medical linear accelerators (linacs) have allowed the clinicians to treat more deep-seated tumors while significantly reduce the dose to the skin (Figure 5(a)). It has also allowed us to shape and deliver the radiation in a way that is more efficient, precise and conform to the tumor. Medical linear accelerators (Figure 5(b)) produce beams of high energy (MeV range) electrons from relatively low energy (about 50 keV) electrons via microwave generated by either a microwave generator (magnetron) or amplifier (klystron). The electrons are accelerated to approximately 95% of speed of light in the accelerator structure. At the end of the accelerator structure, the electrons are bent 270^{o} in a bending magnet and strike a high atomic numbered (Z) target to generate x-rays. The x-rays are filtered by a flattening filter to make the beams uniform in intensity across the field. The beams are initially collimated by a fixed primary collimator and then by the movable jaws in the head of a linac. Additional field shaping is performed by multi-leaf collimators (MLCs), which are made of tungsten and located below the moving jaws. Each leaf can be moved incrementally, and independent of the others, into set positions. The multi-leaf collimators can shape the beams in any arbitrary shape. The leaves are made of tungsten alloy with a thickness of about 7 cm along the beam direction to provide primary x-ray transmission of less than 2% (Khan, 2010).

While the medical linear accelerator is the workhorse of the radiation therapy, there are other treatment machines that can

complement the linac. One system that can accomplish this is the CyberKnife system (Accuray Incorporated, Sunnyvale, CA). It has a linear accelerator mounted on a robotic arm providing 6-MV x-ray beam, which gives better flexibility in the beam positioning due to its compact size and higher degrees of freedom. The Cyberknife system is equipped with an orthogonal x-ray image guidance system to locate the target position during the treatment. It uses three infrared cameras with infrared reflectors for both positioning the patient and tracking the target. It can continuously synchronizes the beam delivery to the tumor motion without the breath hold technique for the patient during the treatment. The synchronization is accomplished by using a correlation model between tumor position, as an internal marker, and the position of external light-emitting diode markers placed on the patient's chest wall (Koong et al., 2004). Based on x-ray images acquired prior to the treatment the correlation model is generated to relate the 3D tumor positions at different phases of the breathing cycle. During treatment, the external marker positions are used to estimate the tumor position and constantly update the system to move the CyberKnife robotic arm according to the target motion. A simulation study has shown that even in the case of irregular breathing patterns the use of internal and external markers allow the robot to accurately follow tumor motion (Seppenwoolde, Berbeco, Nishioka, Shirato, & Heijmen, 2007). Various reports have shown promising results for the early stage lung cancers using CyberKnife for hypofractionated treatments (Bibault et al., 2012; Brown et al., 2007; Chen et al., 2012; Collins et al., 2007; Collins et al., 2009; Vahdat et al., 2010; van der Voort van Zyp et al., 2009). A small sample size study of 37 patients demonstrated that CyberKnife is successful in preserving lung function status as was measured by pulmonary function tests with a better side-effect profile compared to the current standards of care (Agarwal et al., 2012).

TomoTherapy system (TomoTherapy, Inc., Madison, WI) is another system that can complement the linacs. It delivers dynamic helical radiotherapy with imaging guidance using megavoltage computed tomography (MVCT) (Kapatoes et al., 2001; Kapatoes et al., 1999; Mackie et al., 1993; Yang, Mackie, Reckwerdt, Deasy, & Thomadsen, 1997). The radiation unit is a linear accelerator that combines fan beam delivery in a continuously rotating gantry, with

binary multileaf collimators. There is an integrated CT scanner with the treatment machine that allows image acquisition prior to radiation delivery. With megavoltage CT imaging, the soft-tissue can be imaged and daily tumor regression can be documented for patients with non–small-cell lung cancer treated with helical tomotherapy (P. A. Kupelian et al., 2005). The potential efficacy of TomoTherapy system has been shown for early stage lung cancers by sparing of critical structures adjacent to the tumor target (Chi et al., 2011; Zhu & Fu, 2015). Furthermore, it has been shown that the system can achieve dose-per-fraction escalation without increasing the treatment-related morbidity for inoperable non-small cell lung cancer treatment (Monaco et al., 2012; Ramsey, Mahan, Scaperoth, & Chase, 2004)

5. On-Board kilo-voltage Imaging (OBI)

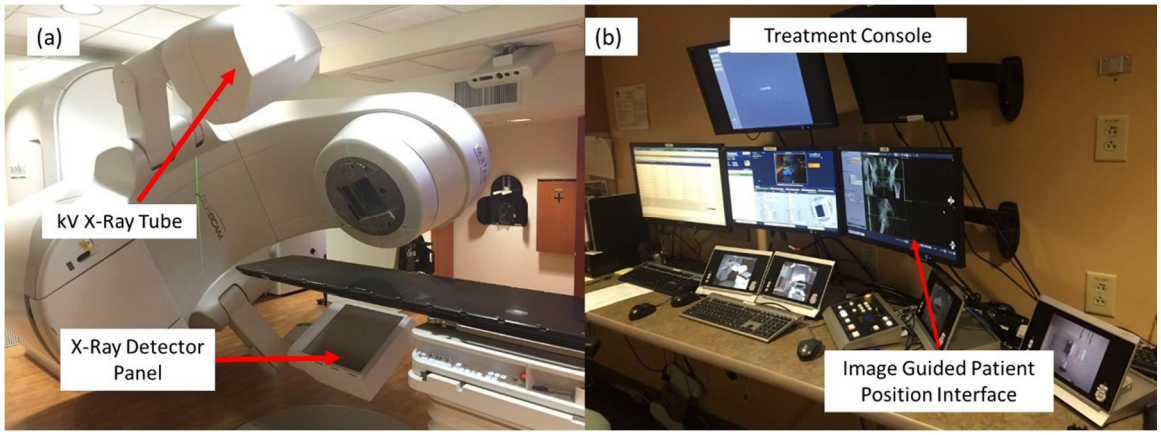

Figure 6. On-board imaging system integrated into a medical linear accelerator. (a) linear accelerator with kV x-ray tube and x-ray detector panel. (b) Treatment console with patient position image registration.

Within the last 15 years, improvements in the x-ray based imaging system integrated into the linear accelerators, also referred as image guided radiation therapy (IGRT), have been a driving force in fast and accurate delivery of radiation to the tumor (Figure 6). This is especially pertinent for lung cancer since it is typically located in an area where there is high image contrast between the tumor and the lung. Historically, mega-voltage (MV) portal imaging was used to verify the target and the patient positioning. Due to the nature of the beams, the MV imaging gives poor image quality especially for soft tissue. Linac-integrated kilo-voltage (kV) imaging

system gives better contrast and high resolution images of soft tissues as well as lower radiation dose than MV portal imaging systems (Mundt & Roeske, 2011). The kV imaging system provides 2-dimensional projection images of the patient/target that can be used in conjunction with digitally reconstructed radiographs (DRR) for target localization and patient setup with respect to the treatment fields (Figure 6(b)).

In addition to the projection images, linac-integrated kV imaging system can acquire cone-beam computed tomography (CBCT) images that are reconstructed from multiple kV projection images acquired during a gantry rotation and provide the three-dimensional images that can be registered with CT image data to improve accuracy in patient positioning (Jaffray, Siewerdsen, Wong, & Martinez, 2002; Sorcini & Tilikidis, 2006).

6. Target Localization and Monitoring Systems

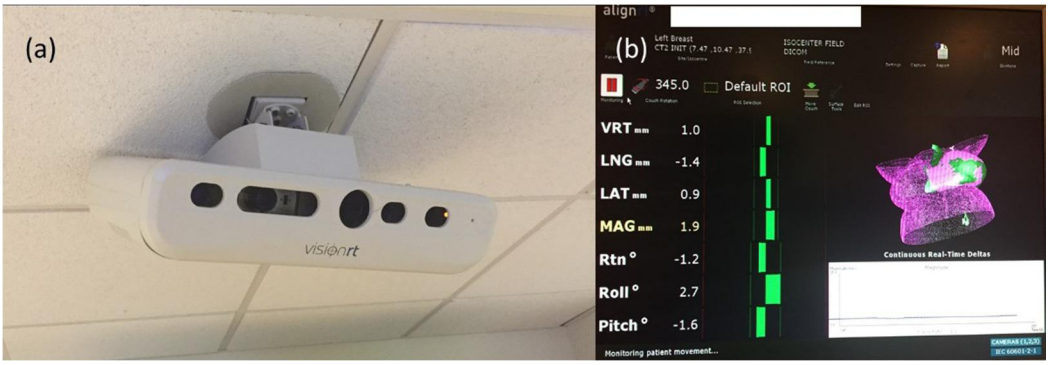

Figure 7. Optical surface tracking system (a) optical camera mounted on the ceiling of the treatment room (see Figures 4(a) and 5) (b) User interface showing patient setup instructions

On-board kV imaging system has greatly improved the accuracy of treatment delivery to the target. However, there have been other technological implementations that facilitated in target localization and real time monitoring of the patient/target. One of the technology is the optical surface tracking system (Figure 7). It typically consists of two or more camera pods providing a real-time 3D surface imaging and determine the position of a patient three dimensionally. Each pod contains one camera that projects a pattern on the patient. The other cameras take images of the reflected pattern. Based on the information from the optical system, the control system would be able to

determine the shifts required to register the patient to the reference images. The optical surface tracking system is typically used in conjunction with an on-board kV imaging system to initially register the patient to the reference images (e.g., CT and DRR) prior to the radiation treatment. Since it is an optics-based monitoring system, it can also track the position of the patient real time during the treatment and provides feedback to the operator if the patient is misaligned during the treatment. It can also be used as a respiratory gating system for breath-hold technique in the thoracic and the abdominal sites (Hughes et al., 2009; Schoffel, Harms, Sroka-Perez, Schlegel, & Karger, 2007).

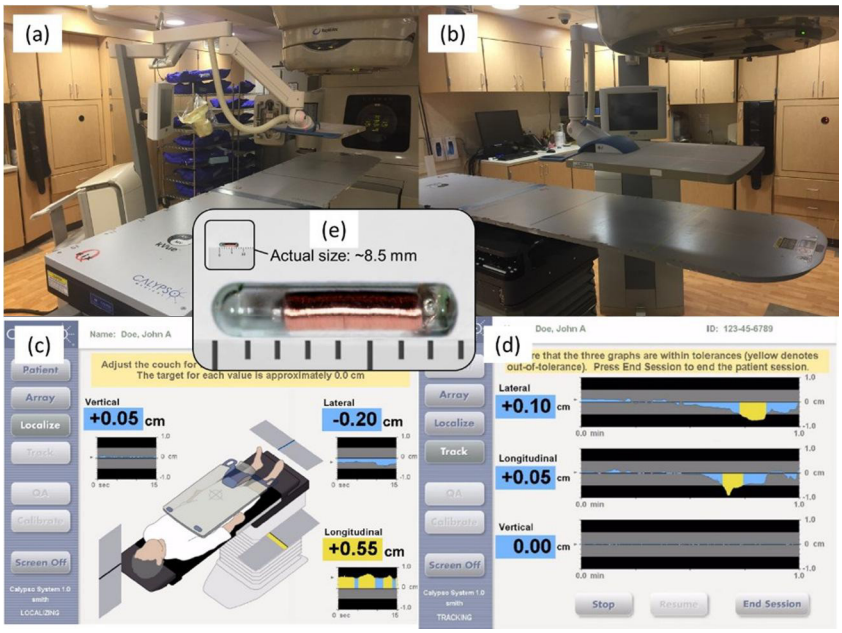

Figure 8. (a) and (b) Electromagnetic tracking system with 4D electromagnetic array, (c) User interface for target localization, (d) User interface for target tracking, and (e) radiofrequency transponder

Other technological implementations for target locations have exploited the concept of using electromagnetic tracking system (Figure 8). An electromagnetic tracking technology uses a radiofrequency transponders implanted in the target (typically in the patient) and track these transponders using a 4D electromagnetic array allowing the clinicians to precisely localize the target prior to the treatment. Furthermore, the transponders can also be tracked real time during the treatment.

Briefly, electromagnetic array is located above the patient target site to emit radiofrequency (RF) signals. The emitted RF signals excite the transponders at their resonant frequencies. The transponders reemit some of the radiofrequency energy in the form of a decaying signal which is detected by the electromagnetic array. The transponder position is then detected relative to the array, which is calibrated to the room coordinate reference system by three rigidly-mounted infrared cameras. One disadvantage of RF tracking systems is that the electromagnetic signals are attenuated by the patient's body and loses intensity of the signal as it traverses through the patient. If the transponders are located in a large patient, the signals may not be high enough to be detected by the electromagnetic array thus cannot track the transponders in real time. The RF tracking systems are most popular for the treatment of prostate cancers (Balter et al., 2005; P. Kupelian et al., 2005; Litzenberg et al., 2007). However, a clinical use and performance of the tracking system in the lung have been investigated (Mayse et al., 2009; M. Mayse et al., 2008; M. L. Mayse et al., 2008; Murphy, Eidens, Vertatschitsch, & Wright, 2008; Parikh et al., 2005).

Other tracking systems have used infrared (IR) tracking technology, similar technology to the 4DCT breathing phase tracking system, in conjunction with x-ray imaging systems. The x-ray system can be either an on-board kV imaging system (Figure 6(a)) or a separate kV imaging system that is mounted on the floor (x-ray tube) and the ceiling (x-ray detector) of the treatment room. It provides fast and highly accurate positioning information by moving the treatment table at the time of treatment. The IR tracking system can monitor the patient position real time and alert the operator if there is a misalignment. Infrared camera system provides a breathing signal by visualizing the motion of IR reflectors placed on the patient surface. The main disadvantage of IR tracking system is that the device provides the external patient motion rather than internal organ or target motion since the reflector block is located on the patient surface. Another potential disadvantage of IR camera tracking is if one reflector is partially or completely blocked by other equipment in the room, it can lead an error in reporting the location of the target. The IR tracking system can also be used for breath hold technique to treat lung lesions (Willoughby et al., 2006). The accuracy and usability of IR cameras to

manage the respiratory motion for tumors in the thorax and abdomen has been verified (Willoughby et al., 2006). Studies have shown that the IR tracking system can monitor the motion of the lung tumor to within 1 mm over all phases of the respiration (Matney, Parker, Neck, Henkelmann, & Rosen, 2011) and reduce the tumor margin (Korreman, Juhler-Nottrup, & Boyer, 2008; Yorke, Rosenzweig, Wagman, & Mageras, 2005).

7. Treatment Techniques

The simplest form of radiation therapy in terms of treatment technique for the treatment of lung cancer is the three-dimensional conformal radiotherapy (3DCRT). In 3DCRT, the treatments are based on a 3D image information from the CT images and deliver a uniform dose that conforms closely to the target while minimizing dose to the critical structures. Typically, two or more beams can be arranged in such a way that all the beams converge at the center of the target. Each field is shaped by a multi-leaf collimator to deliver the radiation uniformly in a static manner. Dose and field sizes will depend of the size of the target and the adjacent critical structures. A typical radiation dose for a late stage lung cancer ranges from 50.4 Gy at 1.8 Gy per fraction to 70 Gy at 2 Gy per fraction. The dose limiting factors is typically the dose received by the critical structures.

Intensity modulated radiation therapy (IMRT) is a treatment technique where a number of different treatment beams with various angles (or continuous arcs) of non-uniform intensity of x-rays optimized by a treatment planning system to deliver a high dose to the target while minimizing dose to the critical structures (Galvin et al., 2004; Liao et al., 2010; Veldeman et al., 2008). A non-uniform intensity of x-ray is achieved by multiple fields and each field is subdivided into a set of subfields irradiated with uniform beam intensity levels. The subfields are created by the MLC and the beams are delivered in a stack arrangement one at a time in sequence without operator intervention. The radiation is turned on and off while the MLC moves to create the next subfield. The total composite of subfield dose delivered creates the intensity-modulated beam.

Stereotactic ablative radiotherapy (SABR) uses IGRT to deliver a high dose to small, deep-seated tumors in the lung (Timmerman, Kavanagh, Cho, Papiez, &

Xing, 2007). Due to the high daily dose delivery, tumor position must be accurately assessed during the treatment. SABR with IGRT will deliver high radiation dose per fraction (typically from 10 Gy to 14 Gy per fraction) for 4 to 5 total fractions to the tumor while sparing normal tissues. SARB is used primarily for stage I inoperable lung cancers with tumor size less than 5 cm in its maximum dimension. Typically 10 to 12 non-opposing narrow (collimated using MLCs), low energy 3DCT are used in lung SABR treatment to maximize the dose to the tumor while avoiding beams entering or exiting through the OARs. IMRT can also be used to achieve the same effect.

8. Proton Therapy

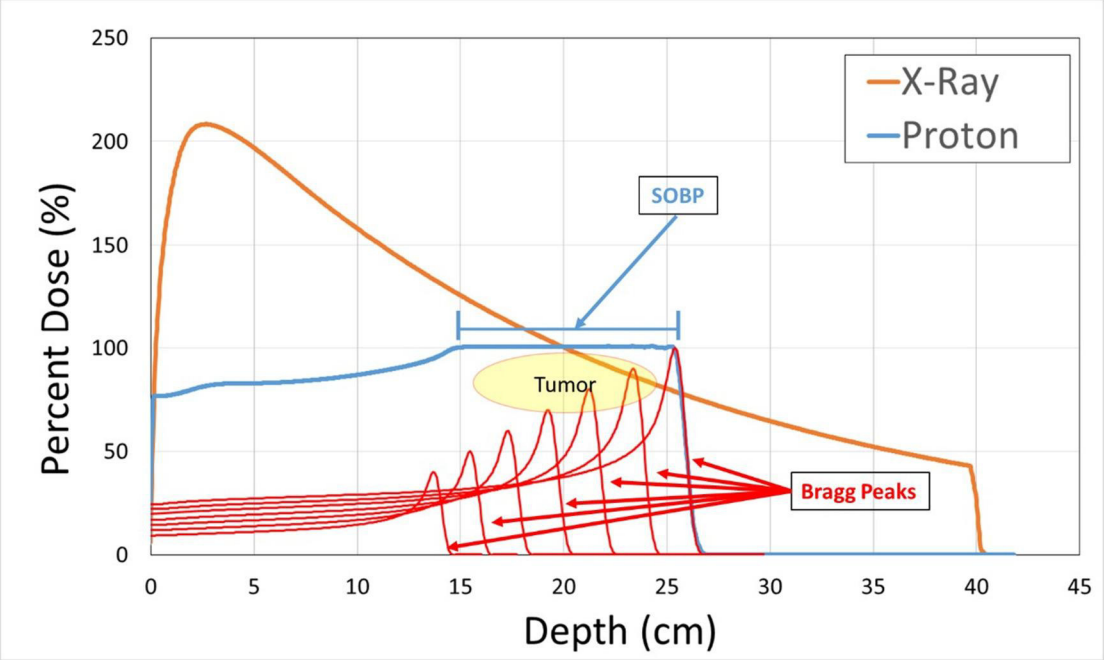

Figure 9. Depth dose distribution comparison of megavoltage x-ray and proton beams. The spread-out Bragg peak is the superposition of several mono-energetic Bragg peaks.

Protons are positively charged sub-atomic particles that are accelerated in either a cyclotron or synchrotron to a kinetic energy of ~240 mega-electron volts (MeV). When mono-energetic protons initially enter a medium (i.e., water), it starts to lose energy with nearby electrons in small increments. As the protons penetrate deeper in the medium, it starts to lose larger amount of energy to its surrounding. Just before it loses

all of its energy, the rate of energy loss peaks and transfers all of its remaining energy. The region in the medium where the maximum energy is lost occurs in a specific depth, which is dependent on the initial energy of the proton beam. This phenomenon is called the Bragg peak (Figure 9). Beyond this point, no radiation energy is imparted in the medium since all of the protons have stopped. When treating a tumor, the goal is to deliver a very uniformly distributed tumoricidal dose deposited by the protons. In order to achieve this, a series of mono-energetic Bragg peaks is delivered to the tumor from high to low energy in order to spread out the Bragg peaks to create a uniformly deposited dose. Typically, the highest energy protons would deposit the most dose and the subsequently lower energy protons would deposit less. This is called the Spread-Out Bragg Peak, SOBP (Figure 9).

Figure 9 is the depth dose distribution comparison between a mega-voltage x-ray and a proton beams. Assuming that the beam (i.e., x-ray and proton) is entering a medium (e.g., water) from left to right, the y-axis would represent the surface. The y-axis is the relative dose where 100% would represent the desired tumoricidal dose (for this illustration, the tumor is located from 15 to 25 cm from the surface). The x-axis is the depth (in cm) penetrated by the beam. The x-ray delivers highest dose at 3.0 cm in the medium and exponentially decreases through the medium. The tumor would receive progressively low dose from the proximal to the distal direction of the radiation. In the end, the radiation would exit out of the medium with some dose. However, the proton beam enters the medium with approximately 75% of dose on the surface and delivers 100% of the desired tumoricidal dose to the entire volume of the tumor and no dose is observed at the distal end of the tumor. With multiple beams, the surface dose is decreased while maintaining uniform dose to the tumor.

In addition to the proton's unique physical characteristics (i.e., no exit dose), it also differs from the x-ray in terms of relative biological effectiveness (RBE). The RBE for proton is generally estimated to be 1.1 times that of x-ray. This means that additional 10% of cancer cells is killed by the proton beams than x-ray beams for the same physical dose.

The primary benefit of using protons to treat cancer compared to x-ray is that there is no

dose distal to the tumor after it has delivered its full dose. This result in a substantially less dose to the critical structures located distal to the tumor. On the other hand, the x-ray beams would deposit dose from the moment it enters the medium and all the way through until it exits the medium. Protons is especially beneficial for the lung cancers that are located medially near the esophagus, heart, and spinal cord.

There have been studies comparing x-ray and protons for the treatment of lung cancer. Nichols *et al.*(Nichols et al., 2011) performed a dosimetric study (study that evaluated the dose distribution using a TPS) for eight stage III non-small cell lung cancer (NSCLC) patients for 3D conformal plans, intensity modulated radiation therapy (IMRT) plans, and proton plans. For all the patients, all three-radiation treatment plans achieved the dose goals for the tumor volumes. Compared against 3D conformal plans, proton plans showed a median reduction of 29% in normal lung V20 (total lung volume receiving > 20 Gy), a median reduction of 33% in mean lung dose (MLD), and a median reduction of 30% for the bone marrow receiving dose > 10 Gy. The V20 and MLD have been reported to be associated with higher risk of radiation pneumonitis (Graham et al., 1999; Jin et al., 2009; Kwa et al., 1998; Wang et al., 2006). The 10 Gy dose to the bone marrow would be sufficient to suppress myelopoiesis within the irradiated marrow. Compared with the IMRT plans, the proton plans offered a median reduction of 26% in normal lung V20, a median reduction of 31% in MLD, and a median reduction of 27% in the volume of bone marrow receiving a dose of > 10 Gy. They concluded that by reducing the volumes of normal structures irradiated, protons can potentially improve the therapeutic index for stage III NSCLC compared to with either 3D conformal or IMRT. Similar results were found by Chang et al (Chang et al., 2006) when they compared the radiation plans that delivered high dose with either protons or x-ray. Proton plans generally reduced the dose to the normal tissues significantly compared with standard-dose x-ray therapy.

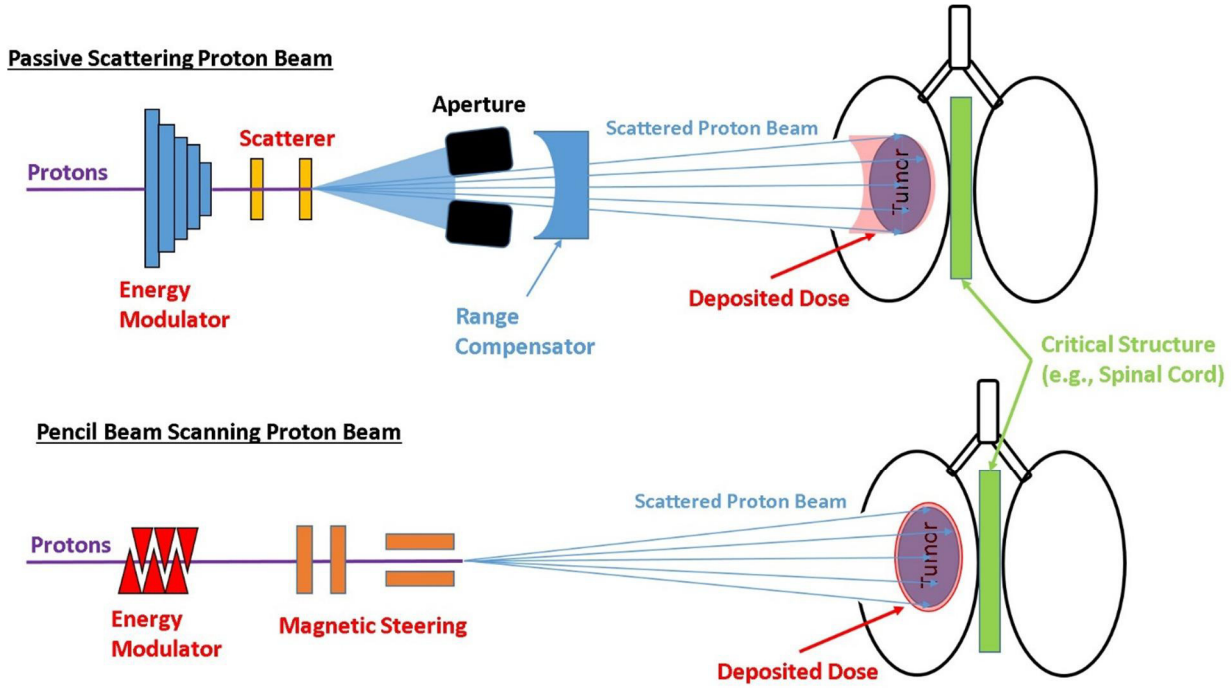

Figure 10. Illustration of passive scattering and pencil beam scanning proton beam systems.

Recently, new proton facilities are installing pencil beam scanning (PBS) systems. The previous proton treatment systems used a passive scattering proton beam where the proton beams are shaped with apertures and range compensators to conform to the distal side of the tumor (Figure 10). PBS systems use a narrow stream of proton beams (i.e., pencil beam) that are scanned within the tumor volume by magnetic fields. The dose to each pencil beams can be adjusted by modulating the intensity of the beam at a point within the tumor volume. The advantage of the PBS system over the passive scattered system is that it can deliver dose to the tumor in a more conformal pattern while significantly reducing neutron contamination that is prevalent in the passive scattered system.

References

Agarwal, R., Saluja, P., Pham, A., Ledbetter, K., Bains, S., Varghese, S., . . . Kim, Y. H. (2012). The effect of CyberKnife therapy on pulmonary function tests used for treating non-small cell lung cancer: a retrospective, observational cohort pilot study. *Cancer Manag Res, 4*, 347-350. doi:10.2147/CMAR.S34194

Ahn, P. H., & Garg, M. K. (2008). Positron emission tomography/computed tomography for target delineation in head and neck cancers. *Semin Nucl Med, 38*(2), 141-148. doi:10.1053/j.semnuclmed.2007.11.002

Ahnesjo, A., & Aspradakis, M. M. (1999). Dose calculations for external photon beams in radiotherapy. *Phys Med Biol, 44*(11), R99-155.

Balter, J. M., Wright, J. N., Newell, L. J., Friemel, B., Dimmer, S., Cheng, Y., . . . Mate, T. P. (2005). Accuracy of a wireless localization system for radiotherapy. *Int J Radiat Oncol Biol Phys, 61*(3), 933-937. doi:10.1016/j.ijrobp.2004.11.009

Barnes, E. A., Murray, B. R., Robinson, D. M., Underwood, L. J., Hanson, J., & Roa, W. H. (2001). Dosimetric evaluation of lung tumor immobilization using breath hold at deep inspiration. *Int J Radiat Oncol Biol Phys, 50*(4), 1091-1098.

Bibault, J. E., Prevost, B., Dansin, E., Mirabel, X., Lacornerie, T., & Lartigau, E. (2012). Image-guided robotic stereotactic radiation therapy with fiducial-free tumor tracking for lung cancer. *Radiat Oncol, 7*, 102. doi:10.1186/1748-717X-7-102

Brown, W. T., Wu, X., Fayad, F., Fowler, J. F., Amendola, B. E., Garcia, S., . . . Schwade, J. G. (2007). CyberKnife radiosurgery for stage I lung cancer: results at 36 months. *Clin Lung Cancer, 8*(8), 488-492. doi:10.3816/CLC.2007.n.033

Chang, J. Y., Senan, S., Paul, M. A., Mehran, R. J., Louie, A. V., Balter, P., . . . Roth, J. A. (2015). Stereotactic ablative radiotherapy versus lobectomy for operable stage I non-small-cell lung cancer: a pooled analysis of two randomised trials. *Lancet Oncol, 16*(6), 630-637. doi:10.1016/S1470-2045(15)70168-3

Chang, J. Y., Zhang, X., Wang, X., Kang, Y., Riley, B., Bilton, S., . . . Cox, J. D. (2006). Significant reduction of normal tissue dose by proton radiotherapy compared with three-dimensional conformal or intensity-modulated radiation therapy in Stage I or Stage III non-small-cell lung cancer. *Int J Radiat Oncol Biol Phys, 65*(4), 1087-1096. doi:10.1016/j.ijrobp.2006.01.052

Chen, V. J., Oermann, E., Vahdat, S., Rabin, J., Suy, S., Yu, X., . . . Collins, B. T. (2012). CyberKnife with Tumor Tracking: An Effective Treatment for High-Risk Surgical Patients with Stage I Non-Small Cell Lung Cancer. *Front Oncol, 2*, 9. doi:10.3389/fonc.2012.00009

Chi, A., Jang, S. Y., Welsh, J. S., Nguyen, N. P., Ong, E., Gobar, L., & Komaki, R. (2011). Feasibility of helical tomotherapy in stereotactic body radiation therapy for centrally located early stage nonsmall-cell lung cancer or lung metastases. *Int J Radiat Oncol Biol Phys, 81*(3), 856-862. doi:10.1016/j.ijrobp.2010.11.051

Collins, B. T., Erickson, K., Reichner, C. A., Collins, S. P., Gagnon, G. J., Dieterich, S., . . . Anderson, E. D. (2007). Radical stereotactic radiosurgery with real-time tumor motion tracking in the treatment of small peripheral lung tumors. *Radiat Oncol, 2*, 39. doi:10.1186/1748-717X-2-39

Collins, B. T., Vahdat, S., Erickson, K., Collins, S. P., Suy, S., Yu, X., . . . Anderson, E. D. (2009). Radical cyberknife radiosurgery with tumor tracking: an effective treatment for inoperable small peripheral stage I non-small cell lung cancer. *J Hematol Oncol, 2*, 1. doi:10.1186/1756-8722-2-1

Curran, W. J., Jr., Paulus, R., Langer, C. J., Komaki, R., Lee, J. S., Hauser, S., . . . Cox, J. D. (2011). Sequential vs. concurrent chemoradiation for stage III non-small cell lung cancer: randomized phase III trial RTOG 9410. *J Natl Cancer Inst, 103*(19), 1452-1460. doi:10.1093/jnci/djr325

Ferlay, J., Steliarova-Foucher, E., Lortet-Tieulent, J., Rosso, S., Coebergh, J. W., Comber, H., . . . Bray, F. (2013). Cancer incidence and mortality patterns in Europe: estimates for 40 countries in 2012. *Eur J Cancer, 49*(6), 1374-1403. doi:10.1016/j.ejca.2012.12.027

Galvin, J. M., Ezzell, G., Eisbrauch, A., Yu, C., Butler, B., Xiao, Y., . . . American Association of Physicists in, M. (2004). Implementing IMRT in clinical practice: a joint document of the American Society for Therapeutic Radiology and Oncology and the American Association of Physicists in Medicine. *Int J Radiat Oncol Biol Phys, 58*(5), 1616-1634. doi:10.1016/j.ijrobp.2003.12.008

Glatstein, E., Lichter, A. S., Fraass, B. A., Kelly, B. A., & van de Geijn, J. (1985). The imaging revolution and radiation oncology: use of CT, ultrasound, and NMR for localization, treatment planning and treatment delivery. *Int J Radiat Oncol Biol Phys, 11*(2), 299-314.

Glide-Hurst, C. K., Schwenker Smith, M., Ajlouni, M., & Chetty, I. J. (2013). Evaluation of two synchronized external surrogates for 4D CT sorting. *J Appl Clin Med Phys, 14*(6), 4301. doi:10.1120/jacmp.v14i6.4301

Graham, M. V., Purdy, J. A., Emami, B., Harms, W., Bosch, W., Lockett, M. A., & Perez, C. A. (1999). Clinical dose-volume histogram analysis for pneumonitis after 3D treatment for non-small cell lung cancer (NSCLC). *Int J Radiat Oncol Biol Phys, 45*(2), 323-329.

Gunderson, L. L., & Tepper, J. E. (2015). *Clinical Radiation Oncology*: Elsevier Health Sciences.

Hughes, S., McClelland, J., Tarte, S., Lawrence, D., Ahmad, S., Hawkes, D., & Landau, D. (2009). Assessment of two novel ventilatory surrogates for use in the delivery of gated/tracked radiotherapy for non-small cell lung cancer. *Radiother Oncol, 91*(3), 336-341. doi:10.1016/j.radonc.2009.03.016

International Commission on Radiation, U., & Measurements. (1999). Prescribing, recording, and reporting photon beam therapy (supplement to ICRU Report 50). *ICRU report, 62*.

Jaffray, D. A., Siewerdsen, J. H., Wong, J. W., & Martinez, A. A. (2002). Flat-panel cone-beam computed tomography for image-guided radiation therapy. *Int J Radiat Oncol Biol Phys, 53*(5), 1337-1349.

Jin, H., Tucker, S. L., Liu, H. H., Wei, X., Yom, S. S., Wang, S., . . . Liao, Z. (2009). Dose-volume thresholds and smoking status for the risk of treatment-related pneumonitis in inoperable non-small cell lung cancer treated with definitive radiotherapy. *Radiother Oncol, 91*(3), 427-432. doi:10.1016/j.radonc.2008.09.009

Kapatoes, J. M., Olivera, G. H., Balog, J. P., Keller, H., Reckwerdt, P. J., & Mackie, T. R. (2001). On the accuracy and effectiveness of dose reconstruction for tomotherapy. *Phys Med Biol, 46*(4), 943-966.

Kapatoes, J. M., Olivera, G. H., Reckwerdt, P. J., Fitchard, E. E., Schloesser, E. A., & Mackie, T. R. (1999). Delivery verification in sequential and helical tomotherapy. *Phys Med Biol, 44*(7), 1815-1841.

Keall, P. J., Mageras, G. S., Balter, J. M., Emery, R. S., Forster, K. M., Jiang, S. B., . . . Yorke, E. (2006). The management of respiratory motion in radiation oncology report of AAPM Task Group 76. *Med Phys, 33*(10), 3874-3900. doi:10.1118/1.2349696

Khan, F. M. (2010). *The physics of radiation therapy* (4th ed.). Baltimore, MD: Lippincott Williams & Wilkins.

Khan, F. M., & Gerbi, B. J. (2011). *Treatment Planning in Radiation Oncology*: Lippincott Williams & Wilkins.

Korreman, S. S., Juhler-Nottrup, T., & Boyer, A. L. (2008). Respiratory gated beam delivery cannot facilitate margin reduction, unless combined with respiratory correlated image guidance. *Radiother Oncol, 86*(1), 61-68. doi:10.1016/j.radonc.2007.10.038

Kupelian, P., Willoughby, T., Litzenberg, D., Sandler, H., Roach, M., Levine, L., . . . Meeks, S. (2005). Clinical experience with the Calypso 4D localization system in prostate cancer patients: implantation, tolerance, migration, localization and real time tracking. *Int J Radiat Oncol Biol Phys. , 63(Suppl 1)*, S197.

Kupelian, P. A., Ramsey, C., Meeks, S. L., Willoughby, T. R., Forbes, A., Wagner, T. H., & Langen, K. M. (2005). Serial megavoltage CT imaging during external beam radiotherapy for non-small-cell lung cancer: observations on tumor regression during treatment. *Int J Radiat Oncol Biol Phys, 63*(4), 1024-1028. doi:10.1016/j.ijrobp.2005.04.046

Kwa, S. L., Lebesque, J. V., Theuws, J. C., Marks, L. B., Munley, M. T., Bentel, G., . . . Ten Haken, R. K. (1998). Radiation pneumonitis as a function of mean lung dose: an analysis of pooled data of 540 patients. *Int J Radiat Oncol Biol Phys, 42*(1), 1-9.

Lee, J. S., Hirsh, V., Park, K., Qin, S., Blajman, C. R., Perng, R. P., . . . Manegold, C. (2012). Vandetanib Versus placebo in patients with advanced non-small-cell lung cancer after prior therapy with an epidermal growth factor receptor tyrosine kinase inhibitor: a randomized, double-blind phase III trial (ZEPHYR). *J Clin Oncol, 30*(10), 1114-1121. doi:10.1200/JCO.2011.36.1709

Levitt, S. H. (2012). *Technical Basis of Radiation Therapy: Practical Clinical Applications*: Springer Science & Business Media.

Li, X. A. (2011). *Adaptive Radiation Therapy*: CRC Press.

Liao, Z. X., Komaki, R. R., Thames, H. D., Jr., Liu, H. H., Tucker, S. L., Mohan, R., . . . Cox, J. D. (2010). Influence

of technologic advances on outcomes in patients with unresectable, locally advanced non-small-cell lung cancer receiving concomitant chemoradiotherapy. *Int J Radiat Oncol Biol Phys, 76*(3), 775-781. doi:10.1016/j.ijrobp.2009.02.032

Litzenberg, D. W., Willoughby, T. R., Balter, J. M., Sandler, H. M., Wei, J., Kupelian, P. A., . . . Pouliot, J. (2007). Positional stability of electromagnetic transponders used for prostate localization and continuous, real-time tracking. *Int J Radiat Oncol Biol Phys, 68*(4), 1199-1206. doi:10.1016/j.ijrobp.2007.03.030

Mackie, T. R., Holmes, T., Swerdloff, S., Reckwerdt, P., Deasy, J. O., Yang, J., . . . Kinsella, T. (1993). Tomotherapy: a new concept for the delivery of dynamic conformal radiotherapy. *Med Phys, 20*(6), 1709-1719. doi:10.1118/1.596958

Mak, D., Corry, J., Lau, E., Rischin, D., & Hicks, R. J. (2011). Role of FDG-PET/CT in staging and follow-up of head and neck squamous cell carcinoma. *Q J Nucl Med Mol Imaging, 55*(5), 487-499.

Matney, J. E., Parker, B. C., Neck, D. W., Henkelmann, G., & Rosen, II. (2011). Target localization accuracy in a respiratory phantom using BrainLAB ExacTrac and 4DCT imaging. *J Appl Clin Med Phys, 12*(2), 3296.

Mayse, M., Peauroi, J., Panikh, P., Misselhorn, D., Dimmer, S., Park, M., . . . Bradely, J. (2009). Long-term interaction and tissue response of a bronchoscopically implanted, anchored electromagnetic transponder in the canine lung. *Int J Radiat Oncol Biol Phys, 75(3)*, S37.

Mayse, M., Smith, R., Park, M., Monteon, G., Silver, E., Parikh, P., . . . Bradley, J. (2008). Development of a non-migrating electromagnetic transponder system for lung tumor tracking *Int J Radiat Oncol Biol Phys, 72(1)*, S430.

Mayse, M. L., Parikh, P. J., Lechleiter, K. M., Dimmer, S., Park, M., Chaudhari, A., . . . Bradley, J. D. (2008). Bronchoscopic implantation of a novel wireless electromagnetic transponder in the canine lung: a feasibility study. *Int J Radiat Oncol Biol Phys, 72*(1), 93-98. doi:10.1016/j.ijrobp.2007.12.055

McCarter, S. D., & Beckham, W. A. (2000). Evaluation of the validity of a convolution method for incorporating tumour movement and set-up variations into the radiotherapy treatment planning system. *Phys Med Biol, 45*(4), 923-931.

Monaco, A., Caruso, C., Giammarino, D., Cianciulli, M., Pressello, M. C., & Donato, V. (2012). Radiotherapy for inoperable non-small cell lung cancer using helical tomotherapy. *Tumori, 98*(1), 86-89. doi:10.1700/1053.11504

Mundt, A., & Roeske, J. (2011). *Image-guided radiation therapy: a clinical perspective*. Shelton: People's Medical Publishing House-USA.

Murphy, M. J., Eidens, R., Vertatschitsch, E., & Wright, J. N. (2008). The effect of transponder motion on the accuracy of the Calypso Electromagnetic localization system. *Int J Radiat Oncol Biol Phys, 72*(1), 295-299. doi:10.1016/j.ijrobp.2008.05.036

Nichols, R. C., Huh, S. N., Henderson, R. H., Mendenhall, N. P., Flampouri, S., Li, Z., . . . Hoppe, B. S. (2011).

Proton radiation therapy offers reduced normal lung and bone marrow exposure for patients receiving dose-escalated radiation therapy for unresectable stage iii non-small-cell lung cancer: a dosimetric study. *Clin Lung Cancer, 12*(4), 252-257. doi:10.1016/j.cllc.2011.03.027

Parikh, P. J., Hubenschmidt, J., Dimmer, S., Vertatschitsch, E., Eidens, R., Wright, J., & Low, D. (2005). 4D verification of real-time accuracy of the Calypso System with lung cancer patient trajectory data. *Int J Radiat Oncol Biol Phys, 63*, S26–S27.

Pawlicki, T., Scanderbeg, D. J., & Starkschall, G. (2016). *Hendee's Radiation Therapy Physics*: John Wiley & Sons.

Ramsey, C., Mahan, S., Scaperoth, D., & Chase, D. (2004). Image-guided adaptive therapy for the treatment of lung cancer. *Int J Radiat Oncol Biol Phys, 60:*, S339.

Rosenzweig, K. E., Hanley, J., Mah, D., Mageras, G., Hunt, M., Toner, S., . . . Leibel, S. A. (2000). The deep inspiration breath-hold technique in the treatment of inoperable non-small-cell lung cancer. *Int J Radiat Oncol Biol Phys, 48*(1), 81-87.

Schoffel, P. J., Harms, W., Sroka-Perez, G., Schlegel, W., & Karger, C. P. (2007). Accuracy of a commercial optical 3D surface imaging system for realignment of patients for radiotherapy of the thorax. *Phys Med Biol, 52*(13), 3949-3963. doi:10.1088/0031-9155/52/13/019

Shen, S., Duan, J., Fiveash, J. B., Brezovich, I. A., Plant, B. A., Spencer, S. A., . . . Bonner, J. A. (2003). Validation of target volume and position in respiratory gated CT planning and treatment. *Med Phys, 30*(12), 3196-3205. doi:10.1118/1.1626121

Simpson, D. R., Lawson, J. D., Nath, S. K., Rose, B. S., Mundt, A. J., & Mell, L. K. (2009). Utilization of advanced imaging technologies for target delineation in radiation oncology. *J Am Coll Radiol, 6*(12), 876-883. doi:10.1016/j.jacr.2009.08.006

Society, A. C. (2015). Cancer facts & figures (pp. v.). Atlanta, GA: The Society.

Sorcini, B., & Tilikidis, A. (2006). Clinical application of image-guided radiotherapy, IGRT (on the Varian OBI platform). *Cancer Radiother, 10*(5), 252-257. doi:10.1016/j.canrad.2006.05.012

Timmerman, R. D., Kavanagh, B. D., Cho, L. C., Papiez, L., & Xing, L. (2007). Stereotactic body radiation therapy in multiple organ sites. *J Clin Oncol, 25*(8), 947-952. doi:10.1200/JCO.2006.09.7469

Vahdat, S., Oermann, E. K., Collins, S. P., Yu, X., Abedalthagafi, M., Debrito, P., . . . Collins, B. T. (2010). CyberKnife radiosurgery for inoperable stage IA non-small cell lung cancer: 18F-fluorodeoxyglucose positron emission tomography/computed tomography serial tumor response assessment. *J Hematol Oncol, 3*, 6. doi:10.1186/1756-8722-3-6

van der Voort van Zyp, N. C., Prevost, J. B., Hoogeman, M. S., Praag, J., van der Holt, B., Levendag, P. C., . . . Nuyttens, J. J. (2009). Stereotactic radiotherapy with real-time tumor tracking for non-small cell lung cancer: clinical outcome. *Radiother Oncol, 91*(3), 296-300. doi:10.1016/j.radonc.2009.02.011

Vedam, S. S., Kini, V. R., Keall, P. J., Ramakrishnan, V., Mostafavi, H., &

Mohan, R. (2003). Quantifying the predictability of diaphragm motion during respiration with a noninvasive external marker. *Med Phys, 30*(4), 505-513. doi:10.1118/1.1558675

Veldeman, L., Madani, I., Hulstaert, F., De Meerleer, G., Mareel, M., & De Neve, W. (2008). Evidence behind use of intensity-modulated radiotherapy: a systematic review of comparative clinical studies. *Lancet Oncol, 9*(4), 367-375. doi:10.1016/S1470-2045(08)70098-6

Wang, S., Liao, Z., Wei, X., Liu, H. H., Tucker, S. L., Hu, C. S., . . . Komaki, R. (2006). Analysis of clinical and dosimetric factors associated with treatment-related pneumonitis (TRP) in patients with non-small-cell lung cancer (NSCLC) treated with concurrent chemotherapy and three-dimensional conformal radiotherapy (3D-CRT). *Int J Radiat Oncol Biol Phys, 66*(5), 1399-1407. doi:10.1016/j.ijrobp.2006.07.1337

Webb, S. (2006). Motion effects in (intensity modulated) radiation therapy: a review. *Phys Med Biol, 51*(13), R403-425. doi:10.1088/0031-9155/51/13/R23

Willoughby, T. R., Forbes, A. R., Buchholz, D., Langen, K. M., Wagner, T. H., Zeidan, O. A., . . . Meeks, S. L. (2006). Evaluation of an infrared camera and X-ray system using implanted fiducials in patients with lung tumors for gated radiation therapy. *Int J Radiat Oncol Biol Phys, 66*(2), 568-575. doi:10.1016/j.ijrobp.2006.05.029

Yang, J. N., Mackie, T. R., Reckwerdt, P., Deasy, J. O., & Thomadsen, B. R. (1997). An investigation of tomotherapy beam delivery. *Med Phys, 24*(3), 425-436. doi:10.1118/1.597909

Yorke, E., Rosenzweig, K. E., Wagman, R., & Mageras, G. S. (2005). Interfractional anatomic variation in patients treated with respiration-gated radiotherapy. *J Appl Clin Med Phys, 6*(2), 19-32.

Zhu, Z., & Fu, X. (2015). The radiation techniques of tomotherapy & intensity-modulated radiation therapy applied to lung cancer. *Transl Lung Cancer Res, 4*(3), 265-274. doi:10.3978/j.issn.2218-6751.2015.01.07